A multifuctional nanoplatform for drug targeted delivery based on radiation-engineered nanogels

Maria Antonietta Sabatino[1], Lorena Anna Ditta[1], Alice Conigliaro[3], Clelia Dispenza[1,3,*]

[1]*Dipartimento dell'Innovazione Industriale e Digitale, Università degli Studi di Palermo, Viale delle Scienze 6, 90128, Palermo Italy*

2 Dipartimento di Biopatologia e Biotecnologie Mediche, Sezione di Biologia e Genetica, Università degli Studi di Palermo, Via Divisi 83, 90133, Palermo, Italy

3 Istituto di Biofisica (IBF), Consiglio Nazionale delle Ricerche, Via Ugo La Malfa 153, 90146, Palermo, Italy

*clelia.dispenza@unipa.it

Abstract

Under a rational design, combining biologically active molecules, ligands to specific cell receptors and fluorescent, radioactive or paramagnetic labels into a single nano-object can bridge the unique properties of the individual components and improve conventional sensing, imaging and therapeutic efficacies. The validation of these functional nano-objects requires careful testing both in terms of physico-chemical properties and biological behaviour *in vitro* and *in vivo*, prior to translation into the clinic. Ionising radiation of aqueous polymer solutions is a viable strategy to produce multifunctional nanogels from aqueous solutions of hydrophilic polymers. By proper selection of the irradiation conditions, polymer concentration and gaseous atmosphere, nanogels with the desired features in terms of dimensions, surface electric charge and chemical reactivity can be produced. In particular, radiation-engineered poly(N-vinyl pyrrolidone)-based nanogels bearing carboxyl groups and primary amines are the core of very promising theranostic nanodevices. The possibility of exploiting these functional groups to bind molecules of interest for their characterisation and biological evaluation is discussed.

Keywords: Nanogels, drug delivery, ionising radiation synthesis, nanomedicine, conjugation reactions.

1. Introduction

Despite the enormous progress in understanding the causes of several important pathologies, such as cancer or neurological diseases, the efficacy of their treatment is limited by the difficulty in delivering the therapeutic molecules to the site of action with the required concentration and temporal modulation. The reasons for inefficient delivery can be related to intrinsic limitations of the therapeutic molecule (poor solubility, chemical instability) and/or to the biological barriers the drug needs to cross to reach the target site. The availability of target-specific nanocarriers that can overcome some of the above limitations represents an important opportunity to improve the current therapeutic strategies. (Cho et al., 2008)

Desirable functions of drug nanocarriers are (i) protection of the drug from degradation or inactivation; (ii) preferential accumulation at the target site; (iii) triggered release or activation of the drug by the action of an internal or external stimulus; (iv) co-delivery of multiple actives; and (v) tracking through non-invasive analyses and bio-imaging approaches. Performing several functions with the same nanodevice is highly attractive but should be achieved without overly increasing the complexity of the nanocarrier and detrimentally affect its commercial scale-up.

Not many comparative studies exist on the various nanomaterials platforms already proposed to control the biodistribution, enhance the efficacy and/or reduce the toxicity of drugs, biologic entities, or imaging agents; neither is there a general agreement on the screening protocols that need to be followed to assess their efficacy. Only in 2017, ISO (the International Organisation for Standardization) has issued a document intended as guidance for "the biological evaluation of medical devices that contain, generate or are composed of nanomaterials". (ISO/TR 10993-22:2017). Toxicological evaluation is critical for the development of any nanomaterial to be used as drug-vector. This means that the empty carrier shall not provoke any injurious biological response at the molecular, cellular or organ level. The carrier should also be degraded into non-toxic degradation products or eliminated through the human excretory system, once completed its task, so to avoid accumulation in tissues and bypass organs. The verification of all these requirements impose several, accurate biological evaluations both *in vitro* and *in vivo*.

According to Bodo et al., in 2016 the FDA-approved nanomedicines were about 50, and 77 products were under clinical trials. Most of the FDA approved materials are polymeric, liposomal, and nanocrystal formulations, while micelles, protein-based NPs and a variety of inorganic and metallic particles are currently in clinical trials. (Bodo et al. 2016; Peer et al. 2007). The more applications one nanocarrier is tested for, the higher becomes the level of confidence in the material properties and the faster and more cost-viable is the process for evaluating its biological safety and therapeutic efficacy.

Nanogels, 3D nanoscalar structures made by crosslinked hydrophilic polymers, are considered very

promising therapeutic nanocarriers. (Kabanov and Vinogradov, 2009) Despite almost 40 years of research, this class of compounds is not yet a commercial product. Some variants are currently under clinical trials, showing promising results. (D'Mello et al., 2017) Likewise other drug nanocarriers, nanogels present limitations regarding the optimization of biodistribution, degradation mechanism and component toxicity. (Neamtu et al., 2017)

Nanogels fall in the blurred boundary between polymeric nanoparticles and hyperbranched polymer chains. They are "open structures", in the sense that they are highly permeable to water molecules and selected solutes, but they are also able to undergo significant conformation transitions in response to environmental changes (stimuli-responsiveness) and thereby they can modify their permeability.

Nanogel size and shape can be fine tuned according to design, but can also change upon a stimulus or in shear fields. This behaviour can facilitate the nanogel extravasation upon intravenous administration, and their elimination. Hendrickson and Lyon demonstrated that the application of a pressure that is comparable to the renal filtration pressure can make nanogels pass through pores that are ten times smaller than their size. (Hendrickson and Lyon, 2010).

Nanogels multi-functionality is another key property since it can provide bio-adhesion features, enable "surface" decoration with targeting ligands, and be exploited for drug loading. The presence of functional groups in the permeable interiors allows drug conjugation without altering too much the surface composition, hence without impacting on colloidal stability or targeting strategies. (Asadian-Birjand et al., 2012) Furthermore, it may ensure drug protection from the body and body protection from potential toxicity of the drug during its systemic transport to the target site. (Picone et al., 2016) Drugs can be loaded by either physical entrapment or by covalent bonding. Using nanogels for physical drug entrapment is not always the most robust approach. If the drug can freely move in, it can also freely move out. The nanoscalar network itself does not represent a diffusional barrier that can grant a sustained release of the incorporated active as in the macroscopic hydrogel delivery systems. Therefore, in order to avoid premature leaking of the loaded active, the network permeability of the nanogel shall be changing during the various phases of drug loading, product storage and administration. This is, indeed, possible if responsive polymers form the polymeric network. (Schmid et al., 2016; Yang et al., 2013)

Covalent binding of drugs to the nanogel by exploitation of its internal and surface functional groups (drug conjugation) can avoid the risk of premature release of the drug. It requires the availability of functional groups in the pharmacologically active molecule that can react in conditions that ensure the required loading without significantly altering the chemical and colloidal stability of the nanovector. The release of the payload at the target site can occur by reactions initiated upon a change

in pH or temperature, due to the presence of enzymes or oxidants and by activation of light or ultrasound. (Adamo et al., 2014; Crucho, 2015; Tong et al., 2014)

Provided that the nanogel possesses sufficient flexibility and depending on the mechanism of action of the biological active agent, drug release is not always required and the nanogel can "expose" the "permanently" conjugated bioactive molecules to the target receptors upon a change of its microenvironment. This has been verified in cell models with nanogels conjugated to oligonucleotides (Dispenza et al., 2014, 2017) and to insulin (Picone et al., 2016, 2018). It should be noted that the conjugation of drugs, imaging agents and targeting ligands on pre-existing particles offers the risk of poorly defined system composition. (Svenson et al., 2013) On the other hand, it grants a higher degree of flexibility in the development of nanocarrier platforms. Moreover, the already FDA-approved nanodrugs are hardly monodisperse or have been individually characterised for their chemical composition. Beside the intra- and inter-individual variability in disease-associated biomarkers, as well as the interpersonal variability in drug response and toxicity, makes the design of the ideal nanodrug still quite arduous.

This short review critically discusses the features of a family of poly(N-vinyl pyrrolidone)-based radiation-synthetised nanogels that have been produced and decorated with various biologically active molecules (Picone et al. 2016, 2018; Dispenza et al. 2017; Adamo et al. 2016a, 2016b) It briefly describes their synthetic process, the origin of their functionalization, the opportunities and limitations of using the functional groups that the nanogels possesses for the conjugation of fluorescent labels required for their characterisation. It also explores the possibility of exploiting these functional groups for the construction of stable, functional hierarchical gels by covalent interlinking.

2. Ionising radiation engineering of nanogel carriers

Nanogels can be produced by irradiation of dilute aqueous polymers or polymer/monomer mixtures with a continuous radiation source (usually a ^{60}Co source) or a pulsed source (generally an electron beam accelerator). (Dispenza et al. 2016a and references herein) Water is the component that absorbs the largest amount of deposited energy and water radiolysis provides a convenient way of initiating polymer radical reactions, also at low temperatures. The radiolysis of water produces a variety of highly reactive species, characterised by oxidizing ($^{\bullet}$OH) or reducing (e^{-}_{aq}, $^{\bullet}$H) properties, which may react with almost any organic substrate. In order to eliminate the contribution of some of the above species, irradiation can be carried out in the presence of gaseous or liquid co-solutes. For example, N_2O saturation transforms the hydrated electrons in hydroxyl radicals, doubling the radiation chemical yield of the latter (G($^{\bullet}$OH)=0.56 µmol/J). (Spinks and Woods, 1990)

The reactive species that initiate radical reactions are mainly hydroxyl radicals. They can undergo (i)

electron transfer; (ii) hydrogen atom abstraction; (ii) addition to double bonds (also to aromatic rings); and addition to electron-rich functional groups. (von Sonntag, 2006)

The advantage of generating hydroxyl radicals through homogeneous radiolysis is that they can form polymer radicals on virtually every polymer chain. The main drawback is that their action will be exerted also towards any (bio)molecular drug or ligand that is dispersed in solution or conjugated to the polymer. This implies that drug loading or nanogel decoration with targeting ligands shall be preferably performed in a separate step, after nanogel synthesis.

Crosslinking is the result of combination reactions between polymer radicals. It is well known that polymer radicals can evolve preferentially towards either crosslinking or scission. (Charlesby and Alexander, 1957) The relative rate constants of the two reactions depend on the chemical structure of the polymer. Irradiation of dilute (crosslinking-type) polymer solutions at high dose-rates favours the simultaneous formation of many radical sites per chain and their intra-molecular combination over inter-molecular combination. This prevents the uncontrolled growth of the network size. (Janik et al., 1997; Ulanski et al., 1994, 1995; Ulanski and Rosiak, 1999) Radicals can also terminate by disproportionation, introducing double bonds in the network. Disproportionation competes with combination and the ratio between the two also depends on the polymer radical structure. (Lazar et al., 1989)

An interesting feature of ionising radiation synthesis of nanogels form dilute polymer solutions is that even starting from polydisperse polymers, fairly monodisperse nanogels can be obtained. Indeed, since a lower number of radicals are formed on the shorter chains than on the longer chains, the shorter chains are more likely to undergo inter-molecular crosslinking while the longer chains are more prone to intra-molecular crosslinking, thus focusing the particle size distribution. (Dispenza et al., 2016b)

In the presence of molecular oxygen, peroxyl radicals are formed from reaction with carbon-centered radicals. Peroxyl radicals further evolve into alkoxyl radicals, which can undergo β-scission forming terminal ketones/aldehydes and alkyl radicals. Under oxidative conditions, ketones/aldehydes can be transformed into carboxyl groups. Interestingly, relatively recently performed studies have shown that molecular oxygen is produced in dilute polymer solutions that were de-aerated prior to irradiation. The accumulated amount of oxygen increases with increasing dose and with decreasing polymer concentration and eventually results in β-scission under initially de-aerated conditions. As the process becomes important only after a certain dose, when a sufficient number of intramolecular crosslinks have already been formed, the size of the nanogel is not significantly affected but the occurrence of low molecular weight products becomes obvious. The rationale for this is the increased formation of hydrogen peroxide at low polymer concentration. In contrast, when molecular oxygen

is present from the beginning, the size of the produced nanogels is smaller than for the same conditions using de-aerated solutions. This is attributed to early β-scission occurring before an intramolecular network of crosslinks has been formed. Under these conditions, reactions between polymer radicals and molecular oxygen will efficiently compete with reactions between polymer radicals. (Ditta et al. submitted)

When scission involves chain segments of already formed networks, it does not have a major impact on nanogel size and molecular weight, since it cleaves bonds of crosslinked chains, but it has a large impact on functionality and reactivity of functional groups, since it transforms the external portions of the network into functionalised dangling chains.

Contrariwise, when molecular oxygen is present from the beginning of the irradiation, its reaction with carbon radicals competes with radical-radical combination and smaller nanogel particles are obtained. Interestingly, under these conditions the amount of generated oxygen is lower and the nanogels are less functionalised. (Ditta et al. submitted)

When unsaturated functionalising monomers are added to the polymer solution, provided that their concentration is sufficiently low and that there is no electric charge interaction between polymer and monomer (strong attraction or repulsion), the addition of the formed polymer radical species to C=C is very fast and occurs with a close to diffusion controlled rate constant. Therefore, we expect the monomer to be grafted to the polymer chain. The radical site is then the transferred to the grafted monomer. Incorporation of charged functional groups may cause charge repulsion between (macro)radicals. This reaction contributes to reduce the yield of intermolecular crosslinking, leading to smaller nanogel particles. (Grimaldi et al., 2014; Adamo et al., 2016a)

In conclusion, varying the polymer solution composition, irradiation conditions (dose-rate and dose) and the composition of the gaseous atmosphere, nanogels of various size and functionalization degree can be produced starting from the same polymer precursor. This makes ionising radiation processing a very interesting approach to engineer nanogel-vectors for delivery applications.

3. Properties of PVP and PVP-co-AA nanogels

A family of poly(N-vinyl pyrrolidone) based nanogels have been synthetised by irradiating aqueous solutions with various polymer and acrylic acid concentrations with a 10 MeV linear accelerator (Elektronika 10/10, ICHTJ Warsaw). The electron pulse length was 4.5 μs and the pulse repetition rate was 300 or 400 Hz. The solutions, previously deareated and saturated with N_2O, were conveyed under the beam via a transporting belt and irradiated with 40 kGy in a single pass at 4°C. (Grimaldi et al., 2014) The nanogels are coded as P*X and P*XAAY, where X is the concentration of polymer in the irradiated solution and Y is the molar ratio between PVP repeating units and acrylic acid. An

overview of systems composition is presented in **Table 1**.

Table 1. Overview of system compositions

System	PVP, wt% (M)	PVP RU, M	AA, M	PVP RU/AA mol ratio
P* 0.1	0.10 (2.44 10^{-6})	9.00 10^{-3}	-	-
P* 0.1AA50	0.10 (2.44 10^{-6})	9.00 10^{-3}	1.8 10^{-4}	50
P* 0.25	0.25 (6.10 10^{-6})	2.25 10^{-2}	-	-
P* 0.25AA50	0.25 (6.10 10^{-6})	2.25 10^{-2}	4.5 10^{-4}	50
P* 0.25AA25	0.25 (6.10 10^{-6})	2.25 10^{-2}	9.0 10^{-4}	25
P* 0.5	0.50 (1.22 10^{-5})	4.50 10^{-2}	-	-
P* 0.5AA50	0.50 (1.22 10^{-5})	4.50 10^{-2}	9 10^{-4}	50

The non-irradiated polymer and the obtained nanogels have been characterised for their average molecular weight and hydrodynamic diameter by static light scattering (SLS) and dynamic light scattering (DLS), respectively. (Sabatino et al., 2013) The surface electric charge has been measured after dialysis. The results are presented in Figure 1. For all systems we observe an increase of weight average molecular weight, thus confirming that no significant chain scission is occurring in the early phase of the process, i.e. before the polymer chains have been involved in multiple crosslinking reactions. The hydrodynamic size of base PVP nanogels increases for polymer concentration equal or higher than 0.25 wt% for the competition between intermolecular and intramolecular crosslinking. In the presence of acrylic acid, combination reactions between polymer radicals compete with addition of acrylic acid to the polymer radical. The most evident effect of this competitive reaction is a much less pronounced increase of nanogel molecular weight and appreciably smaller nanogel particles.

The comparison between the two P*0.5AA50 systems, denoted as P*0.5AA50_1 and P*0.5AA50_2, evidences the effect of pulse frequency; the P*0.5AA50_1 is obtained at a higher frequency than P*0.5AA50_2. If all radiation-induced reactions being initiated during one pulse are completed before the following pulse arrives, no effect of frequency should be appreciated. The fact that, indeed, an effect is present supports the hypothesis that relatively long-lived radicals are formed. We can speculate that, under prolonged irradiation, the hindered segmental mobility of internally crosslinked polymer chains reduces the reactivity of polymer radicals, while the progressively reduced molar concentration of independent polymer chains in the system reduces the probability of their reactive encounters. This, altogether with the possibility of a change of radical structure, from carbon radical to oxyl radical, can explain the observed frequency effect.
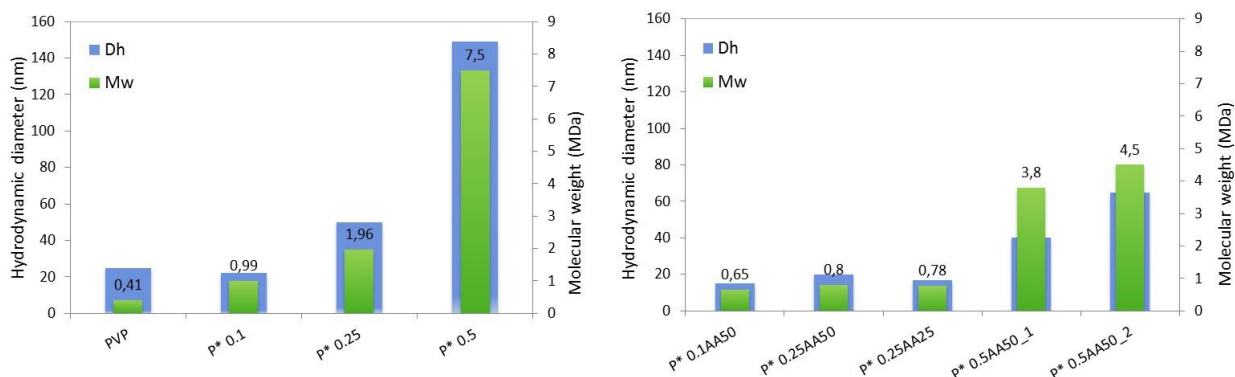
Figure 1. Hydrodynamic diameter from DLS and average weight molecular weight from SLS: non-irradiated polymer and PVP nanogels (left); PVP-co-AA nanogels (right). Irradiation dose is 40 kGy. The error bars represent the width of the distributions. For experimental details see ref. Grimaldi et al., 2014.

Gel filtration chromatography has often been carried out to resolve the distribution of hydrodynamic size of the investigated systems. The chromatograms of selected systems from Table 1 are reported in Figure 2. The lack of polymeric standards with topological features similar to those of nanogels impairs any meaningful quantitative determination of molecular weight distribution curves. Notwithstanding that, the elution curves for the various systems give a better picture of the molecular properties of the nanogels and some further hints on their generation. At first, it can be noticed that the relative positioning of nanogels chromatograms is in accordance with the molecular weight trends from SLS. As already pointed out, all irradiated systems show much narrower distributions than that of linear PVP, especially when nanogels are formed at low polymer concentration. The presence of AA causes a small shift of the chromatograms towards the higher elution volumes (hence smaller hydrodynamic volumes). GFC measurements also support the substantial identity, in terms of molecular properties, of the two carboxyl-functionalized systems obtained for the PVP at 0.25 wt%.
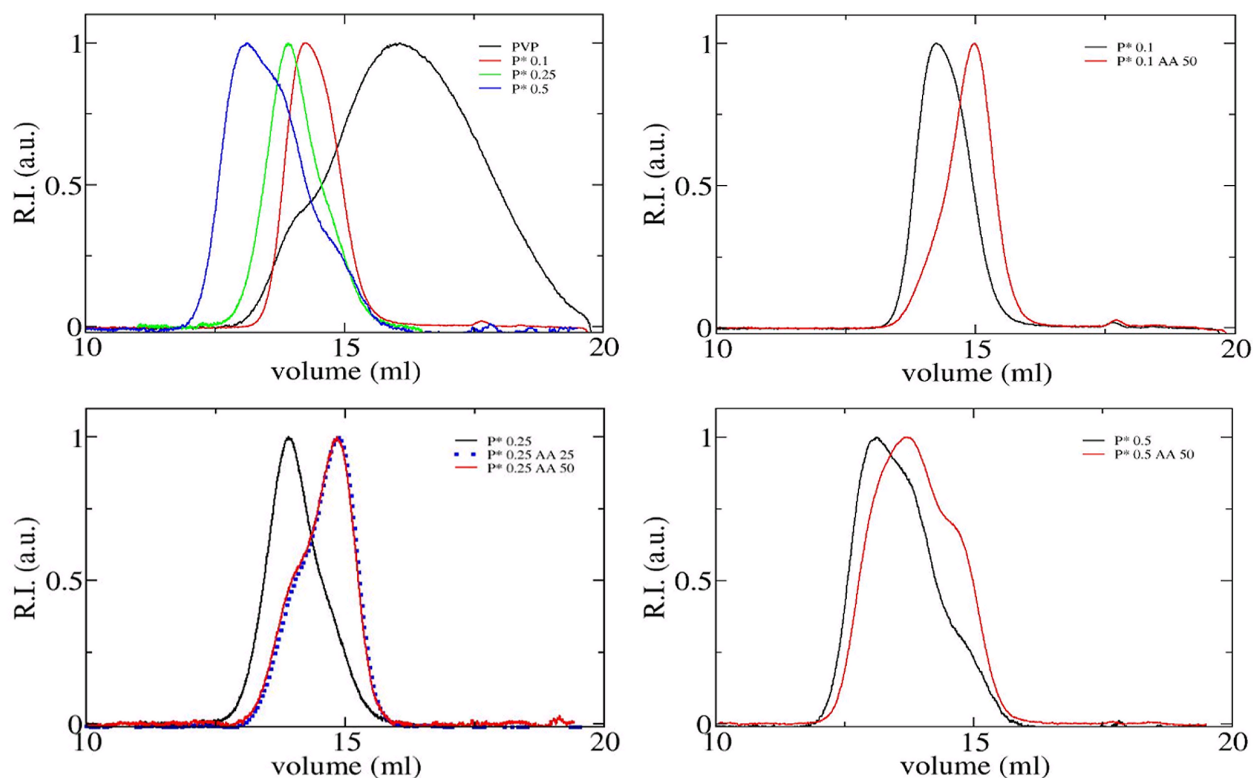
Figure 2: Chromatografic profiles of nanogels produced varying the polymer concentration and adding a small amount of acrylic acid. Base PVP nanogels (top-left); comparison between nanogels produced with and without added AA to the PVP solution: 0.1wt% (top-right); 0.25wt% (bottom-left); 0.5wt% (bottom-right). The chromatogram of the non irradiated polymer is included in the top-left panel as reference. For experimental details see ref. Dispenza et al., 2016b.
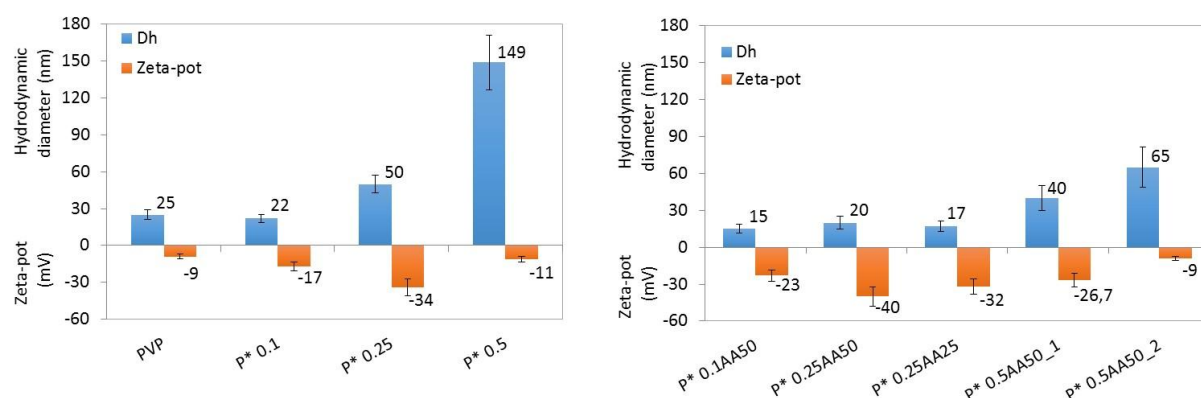

Figure 3. Hydrodynamic diameters and corresponding zeta potential values of PVP (left) and PVP-co-AA (right) nanogels. Irradiation dose is 40kGy. The error bars represent the width of the distributions.

For experimental details on zeta-potential measurements see refs. Dispenza et al., 2012 and Grimaldi et al., 2014.

Some interesting observations can be made looking at the surface charge densities of the nanogels from zeta potential measurements. Ionisable groups, such as carboxyl groups and primary amino groups, are mostly formed upon irradiation, as it has been demonstrated elsewhere. (Dispenza et al., 2016b) They are responsible for the formation of an electric double layer around the nanogel. The zeta potential values, presented in Figure 3, represent the electric potential difference between the slipping plane and the bulk solution. The charges inside the slipping plane move along with the nanogel under the applied electric field. This potential is related to the particle's surface charge density (electric charge per unit of area), both in magnitude and sign, and is independent of particle size. It is generally assumed that colloidal systems with zeta-potential values above 30 mV are stable colloids due to electrostatic repulsion. In the present contest, it should be highlighted that an important contribution to the colloidal stability is steric stabilisation, owing to dangling polymer chains stretching out in the solvent. The zeta-potential of the non-irradiated polymer is only slightly anionic. The anionic character increases for nanogels with respect to linear polymer and, among the nanogels, has a maximum for the systems produced with 0.25 wt% solutions, both with and without AA. From Figure 4, one can appreciate how changing polymer concentration or adding small amounts of acrylic acid allows independent tuning of size and surface electric charge.

It is also interesting to observe how the various systems respond to pH variations of the media. Figure 4 shows zeta-potential values for pure PVP and PVP-co-AA nanogels at various pHs. All systems have been characterised at the same nanogel concentration and various pH, obtained by addition of phosphate buffers (ionic strength 0.2 M). The systems irradiated at 0.1 wt% and 0.5 wt% polymer concentration show similar pH dependence, with a progressively increasing anionic character at the rise of pH, the more for the pure P* nanogels (P*0.1 and P*0.5) compared to the acrylated analogues (P*0.1AA50 and P*0.5AA50). The systems obtained from the irradiation at 0.25wt% solutions show a transition from non-ionic to anionic around the pH that correspond to pKa of monocarboxylic acids, followed by a wide range of zeta potential insensitiveness to pH. The surface charge density has an impact on the yield of the conjugation reactions and nanogel-cell interaction, as will be shown in the following.
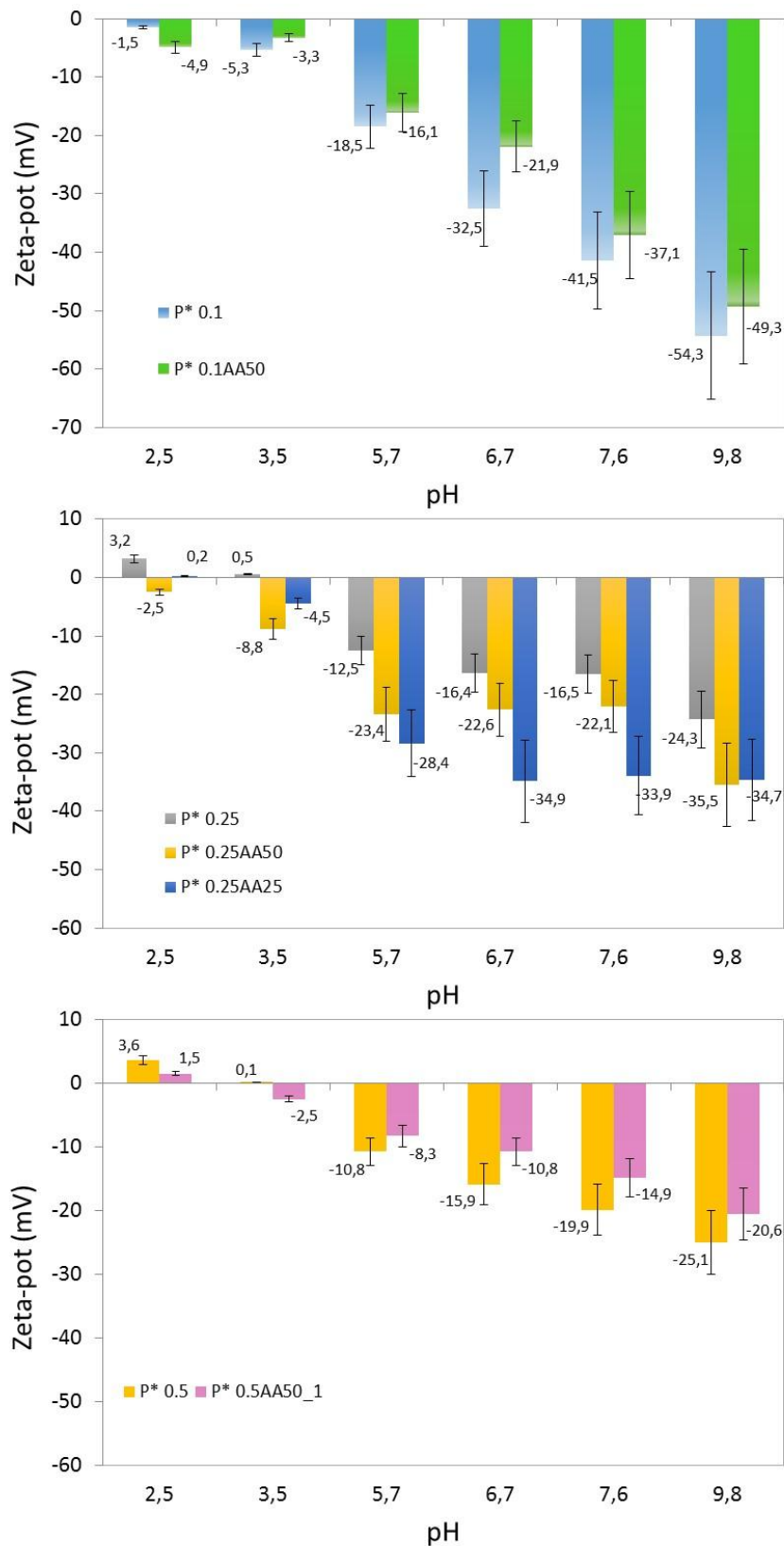
Figure 4. Zeta potential values of PVP and PVP-co-AA nanogels as function of pH. Nanogels produced from 0.1wt% (top), 0.25wt% (middle) and 0.5wt% PVP solutions with and without added acrylic acid. The error bars represent the width of the distributions.

4. Reactions of nanogels with fluorescent labels

The use of nanomaterials in biological applications brings about the need for exploring nanomaterial-cell interactions and evaluate their potential hazard, both *in vitro* and *in vivo*. Fluorescence techniques, including flow cytometry, fluorescence and confocal optical microscopies, are important tools to investigate nanomaterials-cell interactions and nanomaterials biodistribution for their high sensitivity and specificity. Fluorescence based imaging of cells has experienced an enormous increase in resolution that has arrived at the single nanometer scale. (Lv. et al. 2012; Rao et al., 2007)
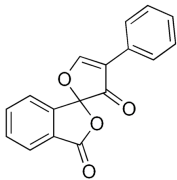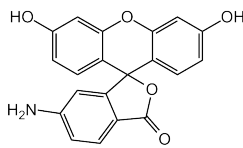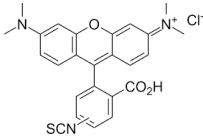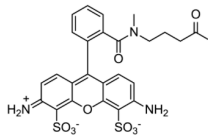
Polymeric nanogels are generally not intrinsically fluorescent, or their inherent fluorescence may not be stable or strong enough to perform the desired evaluations. Therefore, they need to be made fluorescent by adding fluorescent probes. While the use of such labels is indispensible for the studies one is aiming for, labelling implies the risk of perturbation of the nanomaterial properties because of the alteration in chemical composition and/or because of the procedures to load or bind the probe. This means that the probe may change the colloidal stability of the nanogel upon storage or administration, the incorporated drug or ligand functioning mechanism. For this reason, the lowest amount of fluorescent label that enables the nanocarrier visualisation should be used.

Nanogels are generally optically transparent materials; therefore, their colour can be widely tuned by the proper choice of the probe. Yet, colour bleaching and emission peak shifts or attenuations may occur as a result of changes of the local environment of the fluorescent probe. As already pointed out in the introductory chapter, physical entrapment may be an easier strategy than chemical binding, but requires high affinity between probe towards nanogel and present the risk of undesired release. In studies of drug-nanocarrier localisation in cell cultures or biodistribution in animal models, it is of outmost importance that nanogel and probe travel always together. This implies that the binding must resist to all possible changes of its physical and (bio)chemical environment. Covalent attachment generally guarantees the highest stability of the adduct, but it may cause alterations of the emissive properties of the fluorescent molecule.

Fluorescent molecules are also frequently applied for the titration of functional groups and other specific structural and morphological features of hydrogels, proteins and soft matter, in general. Fluorescence spectroscopy exploits the properties of organic molecules whose fluorescent properties change when they bind to specific functional groups (fluorescamine) (Udenfriend et al., 1972), hydrophobic regions (8-anilinonaphthalene-1-sulfonic acid (ANS)), (Haynes and Staerk, 1974) or to specific size cavities (thioflavin-T). (Groenning, 2010) Selected radiation-synthetized nanogels have

been reacted with various fluorescent molecules. In Table 2, fluorescent labels name, molecular structure and conjugation conditions are reported.

Table 2. Fluorescent labels conjugated to radiation-engineered nanogels. Details on the conjugation reactions are provided in the quoted reference.

System	Chemical structure	Molecular weight	Conjugation conditions	Reference
Fluorescamine (FluorA)		278.26	Direct attack to primary amino groups of NG PBS, pH = 7.4	Dispenza et al., 2016
6-amino fluorescein (6-AF)		347	Carbodiimide (EDC), sulfo-NHS ester mediated attack to carboxyl groups of NG MES buffer, pH = 5.5	Adamo et al., 2016a
Tetramethylrhodamine-5-Isothiocyanate (5-TRITC)		443.5	Direct attack to primary amino groups of NG NaHCO$_3$ buffer, pH = 9	Picone et al., 2016
Atto 488, amine modified		858	Carbodiimide (EDC), sulfo-NHS ester mediated attack to carboxyl groups of NG MES buffer, pH = 5.5	as for Atto 633
Atto 633, amine modified	Proprietary	707	Carbodiimide (EDC), sulfo-NHS ester mediated attack to carboxyl groups of NG MES buffer, pH = 5.5	Picone et a., 2018

4.1 Reaction of radiation engineered nanogels with fluorescamine

Fluorescamine (4-phenyl-spiro[furan-2(3H, 1'-phthalan-3,3'-dione) is a fluorescent dye for quantitative determination of primary amines. (Udenfriend et al. 1972) It reacts rapidly with primary amines producing the fluorophore. (see Figure 5) Unreacted fluorescamine hydrolyzes to non-fluorescent products effectively removing it from the reaction, therefore the purification of the conjugate from unreacted dye is not required. Due to its poor water solubility and high reactivity, fluorescamine is added to the samples in a water-miscible nonhydroxylic solvent. Primary amino groups are more reactive towards fluorescamine when they are protonated; for this reason, the reaction is carried out at pH between 7 and 9. When activated with UV light at ca. 390 nm, the dye conjugate has an emission wavelength of approximately 480 nm (green light). The reaction of fluorescamine with the nanogels of Table 1 has been used to quantify primary amino groups and as reference for the conjugation reactions of other molecules of interest to nanogels via its primary amines. The results are reported in Table 3.
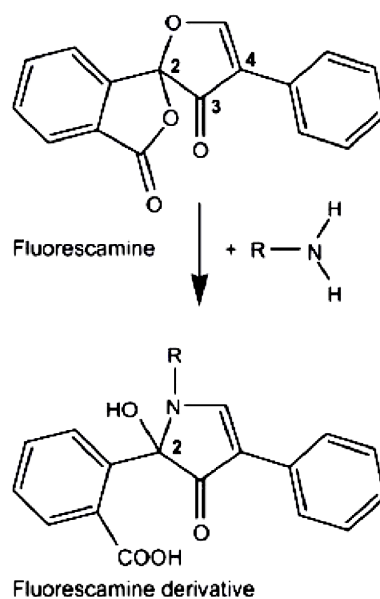

Figure 5. Reaction of non the fluorescent fluorescamine with a primary amine to form a fluorescent adduct.

Table 3. *Degree of conjugation of radiation-engineered nanogels to fluorescamine dye, reported as moles of conjugated fluorescamine per gram of nanogel and per mole of nanogel. The concentration of nanogels (NG) in the reactor is 2.78 10^{-07} M and of fluorescamine (FluorA) is 9.05 10^{-4} M.*

System	FluorA-NG, mol/g	FluorA-NG, mol/mol
P*0.1	4.1 10^{-5}	40
P*0.1AA50	5.4 10^{-5}	35
P*0.25	3.7 10^{-5}	72
P*0.25AA50	2.1 10^{-5}	24
P*0.25AA25	1.8 10^{-5}	15
P*0.5	2.4 10^{-5}	180
P*0.5AA50	2.9 10^{-5}	83

We observe that the concentration of the formed adduct is similar for systems that have been produced from the same polymer concentration, either with or without added acrylic and is highest at the highest polymer concentration. This is in line with other studies carried out on pure PVP nanogels with different irradiation set-ups where it was also observed that the concentration of produced fluorescamine-nanogel adduct increased with the dose at higher polymer concentration, while was dose-independent above 20 kGy for the lower polymer concentration (Dispenza et al. 2016b; Ditta et al. submitted) Admittedly, the mechanism of amino groups formation has not been fully clarified. Yet, these groups can be formed by radiation-induced double scission at the N-C bonds of the pyrrolidone group of PVP, being gamma lactam rings very resistant to hydrolysis at the syntheses pH. The lower amount of adduct detected for nanogels produced at low polymer concentration might reside in the detection method itself. It has been proposed that the fluorescent reaction product of fluorescamine with primary amines is the coplanar and cationic diaryl pyrrolone fluorophore that form upon dehydroxylation from the 2-hydroxyl-pyrrolinone shown in Figure 5. If the carbon atom at position 2 is tetrahedral (as depicted in the figure) the conjugation of the three-ring structure is disrupted and the emission abolished. (Stockert et al., 2008) Therefore, for the amino groups of the nanogels to produce a fluorescent product they need to be accessible and able to host the planar structure of the adduct. Furthermore, dehydroxylation requires the formation of the carboxylate anion, which may be less favoured in anionic networks. Indeed, we have observed that the highest negative

electric charge is observed for the base PVP nanogels produced from more dilute polymer solutions and in the presence of the highest concentration of AA. For these systems, the formation of the quaternary pyrrolone may be difficult.

4.2 Synthesis of fluorescent-labelled radiation engineered nanogels

With the purpose of developing suitable protocols for the synthesis of fluorescent variants of the radiation engineered PVP and PVP-co-AA nanogels for their biological evaluation, but also with the aim of assessing the reactivity of nanogels functional groups towards small molecules with different reactive groups, hydrophilicity and/or electric charge, four fluorescent labels have been reacted with the same nanogel system (P*0.5AA50). This system has on average 67 carboxyl groups and 83 primary amines per nanogel. (Adamo et. al. 2016a) The results in terms of conjugation degree, particle size and surface electric charge after conjugation are reported in Table 4.

4.2.1 Conjugation of TRITC by reaction with nanogel primary amino groups

Tetramethylrhodamine-5 (and 6)-isothiocyanate (TRITC) is a widely used fluorescent label. The isothiocyanate group of TRITC reacts with amines forming a stable carboxamide linkage and a highly fluorescent derivative. The excitation and emission wavelengths are 541 nm and 572 nm, respectively. TRITC demonstrates enhanced stability with respect to FITC (fluorescein isothiocyanate) and is less sensitive to the environmental conditions such as pH (Reeves et al., 2012). The incorporation level of TRITC, similarly to any other fluorescein derivative, has to be optimised. Low incorporation results in low luminescence, while higher levels may cause fluorescein-to-fluorescein quenching effects. For the conjugation to the primary amines of the P*0.5AA50 nanogel, the fluorescent label has been dissolved in DMSO and added to the nanogels in a carbonate buffer at pH 9. The reaction has been carried in a 1:1 molar ratio between fluorescent probe and primary amino groups (estimated using fluorescamine as described above) yielding to ca. 24 probe molecules per nanogel (determined from UV-vis absorption measurements). While the hydrodynamic size of the nanogel is unmodified upon conjugation (66 ± 20 nm), zeta potential changes from -25 ± 6 mV to +5 ± 12 mV, due to the positive charge present on the probe. The concentration of TRITC in the reactor has been reduced ten times to scale-down the amount of probe to 2-3 probe per nanogel and carry out cellular localisation studies, as it will be discussed in the following. The surface charge density is ca. -15 mV.

Table 4. *PVP*0.5AA50 conjugated to various fluorescent molecules: degree of conjugation reported as moles of conjugated probe per gram of nanogel and per mole of nanogel; hydrodynamic diameter*

(nm) and zeta potential (mV) values of probe-nanogel conjugates. The errors for D_H and Zeta-pot represent the widths of the distributions.

System	Probe-NG, mol/g	Probe-NG, mol/mol	D_h, nm	Zeta Pot, mV	Reference
P*0.5AA50	-	-	65 ± 16	-25 ± 6	-
+ TRITC-HC	5.33 10^{-6}	24	66 ± 20	+5 ± 12	Picone et al. 2016
+ TRITC-LC	0.51 10^{-6}	2-3	66 ± 13	-15 ± 9.6	Unpublished
+ 6-AF	1.11 10^{-6}	5	66 ± 16	-17 ± 7.7	Adamo et al. 2016a
+ Atto 633-HC	10.5 10^{-6}	47	68 ± 14	-6.8 ± 6.8	Unpublished
+ Atto 633-LC	0.78 10^{-6}	3-4	67 ± 12	-16.0 ± 5.9	Unpublished
+ Atto 488-LC	0.55 10^{-6}	2-3	74 ± 22	-18.5 ± 7.9	Unpublished

4.2.2 Conjugation of 6-amino fluorescein by reaction with nanogel carboxyl groups

Fluorescein is a well-known green-fluorescent substance with a maximum absorption wavelength at 494 nm and a maximum fluorescence wavelength at 521 nm. There are numerous fluorescein derivatives with different functional groups: fluorescein isothiocynate (FITC) or carboxyfluorescein succinimidyl esters react with amino groups, while 6-aminofluorescein react with activated carboxyl groups. Many of these derivatives have been used in the production of tracers for probing of cell functions, studying drug biodistribution or for angiographic applications. (Brynes et al., US20130165771A1, C. Dive et al., 1988; Graber et al., 1986; Wang et al., 1988)

The amino-derivatized fluorescein variant has been chosen to test the reactivity of EDC/sulfo-NHS activated carboxyl groups of the PVP-co-AA nanogels. (Adamo et al. 2016a, Dispenza et al., 2014) Carbodiimide conjugation works by activating the nanogel carboxyl groups for direct reaction with the primary amine of the probe (added in large excess) via amide bond formation. Because no portion of EDC becomes part of the final bond between conjugated molecules, it is considered a zero-length carboxyl-to-amine crosslinker.
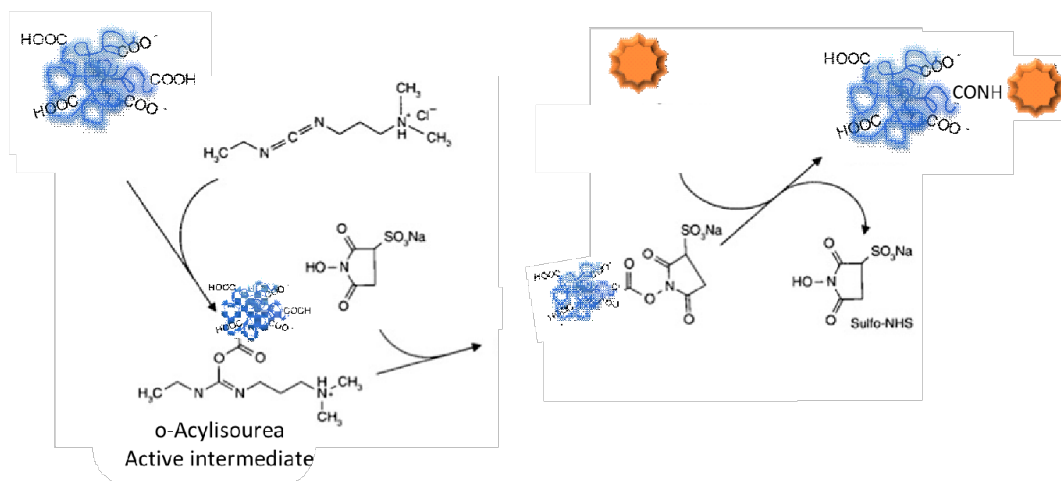
Figure 6. Scheme of EDC/Sulfo-NHS mediated conjugation.

The degree of conjugation reaction for the P*0.5AA50 nanogel is shown in Table 4 and it is about 5 probe molecules per nanogel, significantly lower than the one measured for TRITC. Since the concentration of carboxyl groups in the system has been estimated to be ca. 67 carboxyl groups per nanogel, the paucity of carboxyl groups on the carrier cannot be considered responsible of the low conjugation degree when compared to TRITC and primary amines (83 per nanogel). One possible cause for the low conjugation yield is the low nucleophilicity of the amino group of the probe that is directly bound to the deactivating aromatic ring. Another possibility could be the low efficiency of the EDC/sulfo-NHS activation. On this last aspect, more considerations will be drawn when studying the behaviour of the other amino-functionalised probes (Atto 633 and Atto 488).

From the 6-AF-NG UV-vis absorption spectrum (here not reported), we observe that conjugation causes a significant shift (+ 5 nm) of both absorption and emission peaks of the fluorescent label (Adamo et al., 2016a). This confirms the formation of the amide bond but impairs the direct estimation of the degree of conjugation from the UV-vis absorption at peak. The conjugation degree has been then indirectly estimated from the amount of free probe released through a dialysis membrane. The release experiments, carried out also with the free probe solution and the solution where the nanogels and 6-AF were simply mixed (but not reacted) evidenced that 6-AF can also be physically entrapped into hydrophobic pockets of crosslinked PVP. (Ricca et al., 2010)
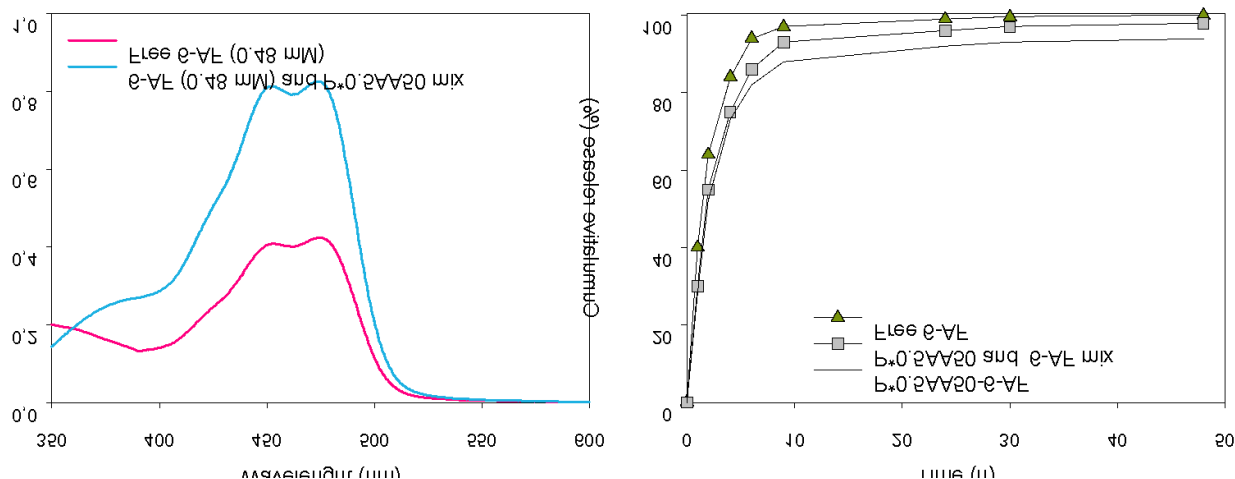
Figure 7: Absorption spectra of 6-AF and P*0.5AA50/6-AF /6-AF solutions (left). Release of 6-AF from dialysis membrane after physical entrapment (P*0.5AA50/6-AF mix) or conjugation (P*0.5AA50-6-AF). The release of free 6-AF is also reported as reference.

The UV-Vis absorption spectra of 6-AF and AF/NG solutions are shown in Figure 7 (left). A reduction in 6-AF peaks absorbance (bleaching) is evident with no peak shift. (Klonis et al., 1998; Song et al., 2001) The release of the probe out of the dialysis membrane when present as the only solute, when mixed with P*0.5AA50 nanogels, and when conjugated to the nanogel are presented in Figure 7 (right). A residual 3.5% of the fluorescent label results physically entrapped, also after prolonged dialysis, while the total amount of the fluorescent molecule retained by the nanogels after conjugation is ca. 10%.

DLS analysis shows that labeling does not affect either the hydrodynamic size or no the surface electric charge density (see Table 4). Despite the low degree of conjugation, AF-NG fluorescent variants have been successfully used for in vitro localization studies of P*0.5AA50 and folic acid-decorated P*0.5AA50 variants with two different cell lines (a positive folate receptor (FR) cell line and a negative FR cell line). Both confocal microscopy and flow cytometric analysis confirm a high degree of internalization (70% after 1h) for the folic acid-decorated variant when incubated with the FR-positive cell line as opposite to the low degree of internalization (15% after 1h) presented when added to the FR-negative cell line. (Adamo et al. 2016a)

4.2.3 Conjugation of Atto488 and Atto633 by reaction with nanogel carboxyl groups

Atto dyes are a relatively new family of fluorescent labels that produce intense fluorescent signals due to strong absorptions and high quantum yields. They are also characterised by high thermal and photostability that make them suitable for *in vivo* applications.

We have selected two dyes, Atto 633 and Atto 488, both in their amino-derivatized form. Atto 633 (λ_{ex} = 633nm, λ_{em} = 651 nm) is characterised by moderate hydrophilicity. Fluorescence is independent of pH (in the range 2 to 11) and after conjugation to the carrier, the label has a net electric charge of +1. Atto 488 (λ_{ex} = 480-515 nm, λ_{em} = 620 nm) is a fluorescent label characterised by higher hydrophilicity and excellent water solubility, due to the presence of both negative and positive electric charges.

For Atto 633, we have initially applied the same reaction protocol used for 6-AF and the degree of conjugation resulted of ca. 47 probe molecules per nanogel. This significantly higher yield supports the hypothesis of the reduced reactivity of the amino group of 6-AF, due to the deactivating contribution of the aromatic ring, and clear up any doubts on the efficiency of the activation by EDC/sulfoNHS activation. The high yield of the conjugation reaction calls for a drastic reduction of the concentration of the probe in the reaction system, since the Atto633-NG conjugate changes the surface electric charge density from negative to almost no charge, which causes formation of aggregates in the cell culture media. By reducing ten times the concentration of Atto633 in the reactor, the conjugation degree was scaled down to 3-4 probe molecules per nanogel. While also for labelling with Atto633, the hydrodynamic size of nanogels is unmodified, the absolute value of the surface charge is reduced.

Performing the same conjugation with Atto488 leads to a lower conjugation degree (2-3 probe molecules per nanogel) probably due to charge repulsion between the slightly anionic nanogels and the sulfonated probe. A ca. 13% increase in size is observed, which might be caused by a slight higher hydration shell.

4.2.4. Comparative analysis of selected fluorescent labelled-nanogels in cell cultures

Localisation in colon cancer cells after 1h and 3h of incubation of fluorescent-labelled P*0.5AA50 nanogels produced with TRITC, Atto633 and Atto488 at low conjugation degree has been investigated by confocal microscopy. Sections at approx. 4.5 μm are shown in Figure 8. The two top panels of Figure 8 refer to red-fluorescent NG-TRITC-LC nanogels. After 1h of incubation, nanogels mostly assemble outside the cell membrane and in the culture medium, while after 3h there is significant evidence of nanogels internalisation with fewer aggregates present outside the cell membrane.

The middle and bottom panels refer to the nanogels conjugated to the two Atto probes at low concentration. We observe that the green NG-Atto488 is mainly localised around the cell membrane both after 1h and 3h conjugation, while NG-Atto633 is mostly present inside the cells, with very few aggregates present in the medium, already after 1h. These results clearly indicate that the choice of

the label affects nanogel-cell interactions, even if the conjugation degree is very low and the average physico-chemical properties of the nanogels do not reveal significant differences among the different systems. This evidence is a warning on the impact that labelling may have on the behaviour of nanocarriers and calls for further investigations.
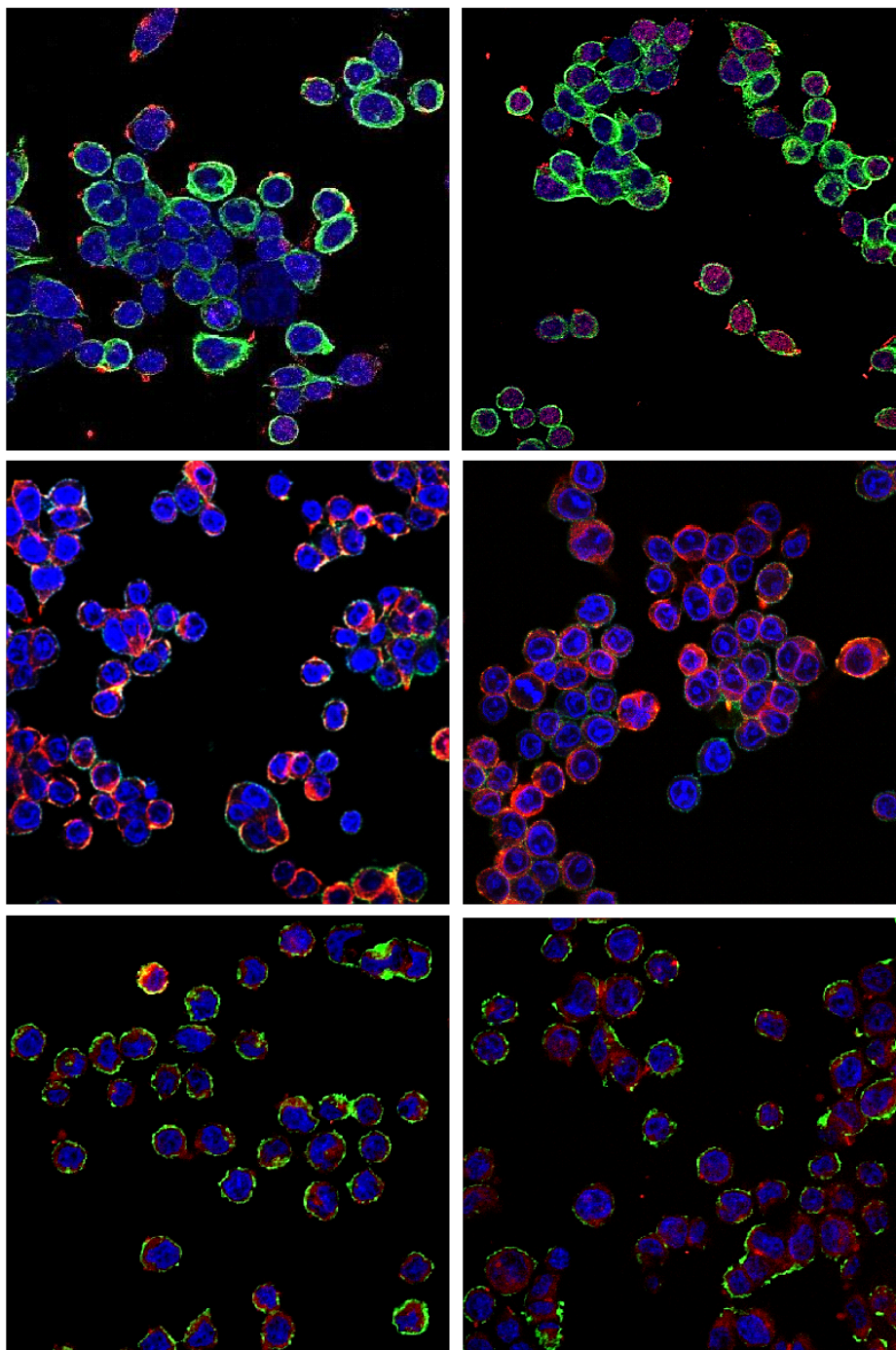

Figure 8. Confocal microscopy sections at ca. 4-5 µm of colon cancer cells (SW480) incubated for 1h (left) and for 3 h (ring) with P*0.5AA50 nanogels conjugated with red fluorescent TRITC (a-b), green fluorescent Atto488 (c-d) and red fluorescent Atto633 (e-f). Nuclei (blue) are stained with

DAPI, cell membrane is stained with green Alexa Fluor[TM] 488 Phalloidin (green, top and bottom panels) or phalloidin (red, middle panels).

5. Covalent nanogel interlinking

The presence of both carboxyl and primary amines in the above-described radiation-engineered PVP nanogels makes their covalent interlinking a possible concurrent reaction when the binding a fluorescent label or any other molecule that requires the activation of nanogels carboxyl groups. Indeed, the activated carboxyl groups can react with the primary amino groups of the same or of another nanogel. The protocols used for labelling nanogels with fluorescent probes have reduced the effect of the concurrent reaction by optimisation of the nanogels concentration and nanogel to probe molar ration in the system. This is not always possible, especially when conjugating therapeutic proteins. The concentration of protein in the system may affect the protein assembly behaviour and, in turn, its structure and function as well as its reactivity. (Wang, 2005) Insulin, for instance, establishes a delicate equilibrium between its monomeric biologically active form and the dimeric and higher oligomeric forms, that depends on concentration, pH, ionic strength, energy and extent of mixing. (Hefford et al., 1986; Kadima et al., 1993; Pekar and Frank, 1972)

On the other hand, covalent crosslinking of nanogels can be pursued for the construction of stable, functional hierarchical gels or coatings through the bottom-up assembly of nanogels as building blocks or for the formation of raspberry-like nano/microparticles. (Sasaki and Akiyoshi, 2012) The advantage is to obtain materials with a well-organised nano-domain structures.

In order to prove that radiation-engineered PVP nanogels can be used as polymerizable nanogel units, we have "activated" the nanogels by addition of EDC and sulfoNHS, without any preliminary concentration of the aqueous dispersion. In Table 5, the hydrodynamic diameters of the nanogels measured before and after activation of their carboxyl groups is shown. The comparison is made using the same volume of nanogel dispersion and the same concentration of catalyst in the reactor. The number of carboxyl groups and primary amino groups are also reported in Table 5. Association is observed for the smaller nanogels with a higher number of carboxyl groups than primary amines per nanogel. Indeed, the smaller particles are present in the reaction volume at relatively higher molar concentration and possess higher diffusivities that favour their mutual reactivity. The imbalance between carboxyl and amino groups in favour of the less reactive carboxyl groups can also be beneficial for their interlinking. For none of the formulations we observed reduction of hydrodynamic size, which suggests that further intra-molecular crosslinking is not likely to occur.

Table 5. Hydrodynamic diameters of PVP and PVP-co-AA nanogels before and after interlinking, by activation of their carboxyl groups, following the protocol described in Adamo et al., 2016a. The errors for D_h represent the width of the distributions.

System	COOH, mol/mol	NH$_2$, mol/mol	D_H, nm	
			Before	After
P*0.1	111	49	22 ± 10	64 ± 37
P*0.1AA50	71	35	15 ± 9	52 ±26
P*0.25	14	72	50 ±14	50 ±16
P*0.25AA50	19	24	20 ± 9	30 ± 15
P*0.25AA25	28	15	17 ± 10	90 ± 40
P*0.5	1	180	149 ± 45	150 ± 42
P*0.5AA50	67	83	65 ± 16	66 ± 12

The base P*X nanogels have been also activated in the presence of a small molar concentration of FITC-labelled insulin (10 μM, PBS, pH 7.4), following the same protocol described in Picone et al. 2016. Atto633 was also conjugated to one of the systems as (13 μM, MES, pH 5.5), as described in Picone et al. 2018. In Table 6, the results in terms of nanogels hydrodynamic size and conjugation degree are reported. In this case, the smaller P*0.1 nanogels increase even more markedly their hydrodynamic size, showing a highly polydisperse size distribution. This behaviour may suggest that is actually bridging nanogels together. The P*0.25 confirms its low propensity in reactive aggregation. Interestingly, P*0.5 has the highest conjugation degree, yet shows a significant reduction of hydrodynamic size, which may suggest the occurrence of insulin-mediated intra-particle crosslinking. The same system, reacted with an excess of Atto633 probe, does not change its hydrodynamic size, thus supporting the role of the multifunctional protein in the network rearrangement.

Tab 6. Hydrodynamic diameter (D_H) and degree of conjugation of FITC-labeled insulin and Atto633 to base PVP nanogels. The errors for D_h represent the width of the distributions.

NG conjugated system	D_H (nm)	CD (μmol/g pol)
NG(0.1)-Ins[FITC]	>100 nm multimodal	0.04
NG(0.25)-Ins[FITC]	57 ± 17	0.04
NG(0.5)-Ins[FITC]	84 ± 21	0.08
NG(0.5)-Atto633	147 ± 41	0.5

Conclusions

Nanogels are fascinating drug delivery systems that can play an important role in addressing some of the issues related to diagnosis and treatment of a wide range of diseases. Nanogels synthetized by high energy irradiation are very interesting nanoconstructs where size and chemical functionality can be fine tuned starting from the same polymer precursor, by an appropriate choice of the irradiation conditions, polymer concentration and gaseous atmosphere. In particular, pulsed ebeam irradiation of deareated aqueous poly(N-vinyl pyrrolidone) solutions transform the polydisperse and inert chains into nanogels characterized by suitable sizes for their use as nanocarriers and reactive carboxyl groups and primary amines. It has been shown how these functionalities play a key role in the modification of nanogel through the covalently attachment of (bio)molecules of interest, from fluorescent probes required for their in vitro and vivo evaluation to therapeutic proteins. It has also been demonstrated that they can be used to transform individual nanogel particles into larger raspberry-like particles. It is also evident that even a very minute modification of nanogels structure and network organisation by reactive coupling with more or less hydrophilic or charged molecules may have an impact on their interaction with biological systems. This evidence represents a warning for careful and robust design of biological experiments.

References

Adamo, G., Grimaldi, N., Campora, S., Bulone, D., Bondì, M.L., Al-Sheikhly, M., Sabatino, M.A., Dispenza, C., Ghersi, G., 2016a. Multi-Functional Nanogels for Tumor Targeting and Redox-Sensitive Drug and siRNA Delivery. Molecules, 23, 1594.

Adamo, G., Grimaldi, N., Sabatino, M.A., Walo, M., Dispenza, C., Ghersi, G., 2016b. E-beam crosslinked nanogels conjugated with monoclonal antibodies in targeting strategies. Biol. Chem. 398(2), 277-287.

Adamo, G., Grimaldi, N., Campora, S., Sabatino, M.A., Dispenza, C., Ghersi, G., 2014. Glutathione-Sensitive Nanogels for Drug Release. Chem. Eng. Trans. 38, 457-462.

Asadian-Birjand, M., Sousa-Herves, A., Steinhilber, D., 2012. Functional nanogels for biomedical applications. Curr Med Chem. 19, 5029–43.

Bobo, D., Robinson, K.J., Islam, J., Thurecht, K.J., Corrie, S.R., 2016. Nanoparticle-Based Medicines: A Review of FDA-Approved Materials and Clinical Trials to Date. Pharm. Res. 33(10), 2373-2387. doi: 10.1007/s11095-016-1958-5.

Brynes, P. J., et al., U. S. Patent No. 4,869,132

Charlesby, A., Alexander, P., 1957. Effect of X-rays and γ-rays on synthetic polymers in aqueous solution. J. Polym. Sci., 23, 355-375.

Cho, K., Wang, X., Nie, S., Chen, Z.G., Shin, D.M., 2008. Therapeutic Nanoparticles for Drug Delivery in Cancer. Clin Cancer Res. 14(5), 1310-1316.

Crucho, C., 2015. Stimuli-responsive polymeric nanoparticles for nanomedicine. Chem Med Chem. 10, 24–38.

Dispenza, C., Sabatino, M.A., Grimaldi, N., Bulone, D., Bondi, M.L., Casaletto, M.P., Rigogliuso, S., Adamo, G., Ghersi, G., 2012. Minimalism in Radiation Synthesis of Biomedical Functional Nanogels. Biomacromolecules. 13, 1805–1817.

Dispenza, C., Adamo, G., Sabatino, M.A., Grimaldi, N., Bulone, D., Bondi, M.L., Rigogliuso, S., Ghersi, G., 2014. Oligonucleotides-decorated-poly(*N*-vinyl pyrrolidone) nanogels for gene delivery. J. Appl. Polym. Sci. 131, 39774.

Dispenza, C., Spadaro G., Jonsson M. Radiation Engineering of Multifunctional Nanogels. Top Curr Chem (Z), 2016a, 374, 69.

Dispenza, C., Sabatino, M.A., Grimaldi, N., Mangione, M. R., Walo, M., Murugand, E., Jonsson, M., 2016b. On the origin of functionalization in one-pot radiation synthesis of nanogels from aqueous polymer solutions. RSC Adv. 6, 2582–2591.

Dispenza, C., Sabatino, M.A., Ajovalasit, A., Ditta, L.A., Ragusa, M., Purrello, M., Costa, V., Conigliaro, A., Alessandro, R., 2017. Nanogel-antimiR-31 conjugates affect colon cancer s behaviour. RSC Adv. 7(82), 52039-52047.

Dive, C., Cox, H., Watson, J.V., Workman, P., 1988. Polar fluorescein derivatives as improved substrate probes for flow cytoenzymological assay of cellular esterases. Mol. Cell. Probes. 2(2), 131-145.

Ditta, L.A., Dahlgren, B., Sabatino, M.A., Dispenza, C., Jonsson M., Understanding generation of multifunctional nanogels in chemical-free one-pot synthesis. Submitted.

D'Mello, S.R., Cruz, C.N., Chen, M.-L., Kapoor, M., Lee, S.L., Tyner, K.M., 2017. The evolving landscape of drug products containing nanomaterials in the United States. Nat. Nanotechnol.12, 523–529.

Graber, M.L., DiLillo, D.C., Friedman, B.L., Pastoriza-Munoz, E., 2012. Characteristics of fluoroprobes for measuring intracellular pH. Anal Biochem.156, 202–212.

Grimaldi, N., Sabatino, M.A., Przybytniak, G., Kaluska, I., Bondì, M.L., Bulone, D., Alessi, S., Spadaro G., Dispenza, C., 2014. High-energy radiation processing, a smart approach to obtain PVP-graft-AA nanogels. Radiat. Phys. Chem. 9, 76–79.

Groenning, M., 2010. Binding mode of Thioflavin T and other molecular probes in the context of amyloid fibrils—current status. J Chem Biol. 3(1), 1–18.

ISO/TR 10993-22:2017. Biological evaluation of medical devices – Part 22: Guidance on nanomaterials.

Haynes D. H., Staerk, H., 1974. 1-Anilino-8-naphthalenesulfonate: A fluorescent probe of membrane surface structure, composition and mobility. The J. Membr. Biol. 17(1), 313–340.

Hefford, M.A., Oda, G., Kaplan, H., 1986. Structure-function relationships in the free insulin monomer. Biochem J. 237, 663–668.

Hendrickson, G.R., Lyon, L.A., 2010. Microgel translocation through pores under confinement. Angew Chem Int Ed. 49, 2193–2197.

Janik, I., Kujawa, P., Ulanski, P., Rosiak, J.M., 1997. Pulse radiolysis of polymers in aqueous solution. Kinetics study. J. Chim. Phys. 94, 244-250.

Kabanov, A.V., Vinogradov, S.V., 2009. Nanogels as pharmaceutical carriers: finite networks of infinite capabilities. Angew. Chem. Int. Ed. Engl. 48(30), 5418–5429.

Kadima, W., Ogendal, L., Bauer, R., Kaarsholm, N., Brodersen, K., Hansen, J.F., Porting, P., 1992. The influence of ionic strength and pH on the aggregation properties of zinc-free insulin studied by static and dynamic laser light scattering. Biopolymers. 33, 1643–1657.

Klonis, N., Clayton, A.H.A., Voss Jr., E.W., Sawyer, W.H., 1998. Spectral properties of fluorescein in solvent-water mixtures: applications as a probe of hydrogen bonding environments in biological systems. Photochem. Photobiol. 67, 500-510.

Lazar, M., Rychly, J., Klimo, V., Pelikan, P., Valko, L., 1989. Free Radicals In Chemistry and

Biology. CRC Press Boca Raton Florida.

Lv, Y., Liu, M., Zhang, Y., Wang, X., Zhang, F., Li, F., Bao, W., Wang, J., Zhang, Y., Wei, W., Ma, G., Zhao, L., Tian, Z., 2018. Cancer Cell Membrane-Biomimetic Nanoprobes with Two-Photon Excitation and Near-Infrared Emission for Intravital Tumor Fluorescence Imaging. ACS Nano. 12(2), 1350-1358.

Neamtu, I., Rusu, A.G., Diaconu, A., Nita, L.E., Chiria A.P., 2017. Basic concepts and recent advances in nanogels as carriers for medical applications. Drug Deliv. 24(1), 539–557.

Pekar, A.H., Frank, B.H., 1972. Conformation of proinsulin. A comparison of insulin and proinsulin self-association at neutral pH. Biochemistry. 11, 4013–4016.

Peer, D., Karp, J.M., Hong, S., Farokhzad, O.C., Margalit, R., Langer, R., 2007. Nanocarriers as an emerging platform for cancer therapy. Nat. Nanotecnol. 2(12), 751-60. doi: 10.1038/nnano.2007.387.

Picone, P., Ditta, L.A., Sabatino, M.A., Militello, V., San Biagio, P.L., Di Giacinto, M.L., Cristaldi, L., Nuzzo, D., Dispenza, C., Giacomazza D., Di Carlo, M., 2016. Ionizing radiation-engineered nanogels as insulin nanocarriers for the development of a new strategy for the treatment of Alzheimer's disease. Biomaterials. 80, 179–194.

Picone, P., Sabatino, M.A., Ditta L.A., Amato, A., San Biagio, P.L., Mulè, F., Giacomazza, D., Dispenza, C, Di Carlo M., 2018. Nose-to-brain delivery of insulin enhanced by a nanogel carrier. J Control. Rel. 270, 23-36.

Rao, J., Dragulescu-Andrasi, A., Yao, H., 2007. Fluorescence imaging in vivo: recent advances. Curr Opin Biotechnol. 18(1), 17-25.

Reeves, K.J., Brookes, Z.L.S., Reed, M.W.R., Brown N.J., 2012. Evaluation of Fluorescent Plasma Markers for in vivo Microscopy of the Microcirculation. J Vasc Res. 49, 132–143. DOI:10.1159/000331281.

Ricca, M., Foderà, V., Giacomazza, D., Leone, M. Spadaro, G., Dispenza, C., 2010. Probing the internal environment of PVP networks generated by irradiation with different sources. Colloid Polym. Sci. 288, 969–980.

Rosiak, J. M., Ulanski, P., 1999. Synthesis of hydrogels by irradiation of polymers in aqueous solution. Radiat Phys Chem. 55, 139-151.

Sabatino, M.A., Bulone, D., Veres, M., Spinella, A., Spadaro, G., Dispenza, C., 2013. Structure of e-beam sculptured poly (N-vinylpyrrolidone) networks across different length-scales, from macro to nano. Polymer. 54(1), 54–64.

Sasaki, Y., Akiyoshi, K., 2012. Self-assembled Nanogel Engineering for Advanced Biomedical Technology. Chem. Lett. 41(3), 202-208.

Schmid, A.J., Dubbert, J., Rudov, A.A., Pedersen, J. S., Lindner, P., Karg, M., Potemkin, I.I., Richtering, W., 2016. Multi-Shell Hollow Nanogels with Responsive Shell Permeability. Scientific Reports. 6, 22736; doi :10.1038/srep22736.

Song, A., Zhang, J., Zhang, M., Shen, T., Tang, J., 2000. Spectral properties and structure of fluorescein and its alkyl derivatives in micelles. Colloids Surf., A 167: 253-262.

Spinks J. W., Woods R. J., An Introduction to Radiation Chemistry. third ed. 1990, New York: John Wiley and Sons, Inc.

Stockert, J. C., Blazquez, A., Galaz, S., Juarranz, A., 2008. A mechanism for the fluorogenic reaction of amino groups with fluorescamine and MDPF. Acta Histochem. 110(4), 333-340.

Svenson, S., 2013. Theranostics: Are We There Yet? Mol. Pharmaceutics. 10(3), 848–856.

Tong, R., Tang, L., Ma, L., Tu, C., Baumgartner, R., Cheng, J., 2014. Smart chemistry in polymeric nanomedicine. Chem Soc Rev. 43, 6982–7012.

Udenfriend, S., Stein, S., Bohlen, P., Dairman, W., Leimgruber W., Weigele, M., 1972. Fluorescamine: A reagent for Assay of amino acids, Peptides, Proteins and Primary Amines in the Picomole Range. Science. 178, 871-872.

Ulanski, P., Bothe, E., Rosiak, J.M., von Sonntag, C., 1994. OH radical-induced crosslinking and strand breakage of poly(vinyl alcohol) in aqueous solution in the absence and presence of oxygen. A pulse radiolysis and product study. Macromol. Chem. Phys. 195(4), 1443-1461.

Ulanski, P., Zainuddin, & Rosiak, J.M., 1995. Pulse radiolysis of poly(ethylene oxide) in aqueous solution. II. Decay of macroradicals. Radiat. Phys. Chem. 46(4-6), 917-920.

Ulanski, P., Rosiak, J.M., 1999. The use of radiation technique in the synthesis of polymeric nanogels. Nucl. Instr. and Meth. in Phys. Res. B. 151, 356-360.

von Sonntag, C. 2006. Free-radical-induced DNA damage and its repair. Berlin, Heidelberg, New York: Springer-Verlag.

Wang N. Y., et al., European Patent Application Publ. No. EP264797 (1988)

Wang W. 2005. Protein aggregation and its inhibition in biopharmaceutics. Int. J. Pharm. 289, 1–30.

Yang, H. M., Lee, H. J., Kim, J. D., 2013. Core–shell nanogel of PEG–poly(aspartic acid) and its pH-responsive release of rh-insulin. Soft Matter. 9(6), 1781–1788.